Mean-field dynamics of the superfluid-insulator phase transition in a gas of ultracold atoms

Jakub Zakrzewski
Instytut Fizyki imienia Mariana Smoluchowskiego and Mark Kac Complex Systems Research Center, Uniwersytet Jagielloński, ulica Reymonta 4, PL-30-059 Kraków, Poland
(Received 8 June 2004; published 4 April 2005)

A large-scale dynamical simulation of the superfluid–Mott-insulator transition in a gas of ultracold atoms placed in an optical lattice is performed using the time-dependent Gutzwiller mean-field approach. This approximate treatment allows us to take into account most of the details of the recent experiment [Greiner *et al.*, Nature (London) **415**, 39 (2002)] where by changing the depth of the lattice potential an adiabatic transition from a superfluid to a Mott insulator state has been reported. Our simulations reveal a significant excitation of the system with a transition to insulator in restricted regions of the trap only.

DOI: 10.1103/PhysRevA.71.043601 PACS number(s): 03.75.Kk, 03.75.Lm

I. INTRODUCTION

The theoretical suggestion [1] of the possibility of realizing one of the standard models for interacting particles—the Bose-Hubbard (BH) model [2,3]—in a cold gas placed in an optical lattice was followed soon by a seminal experiment [4]. The reported realization of a quantum phase transition between superfluid (SF) and Mott insulator (MI) phases showed convincingly that it was possible to control experimentally the parameters of the model practically at will. This triggered several studies involving Bose condensates [5–10] as well as, more recently Fermi-Bose mixtures [11–13] placed on optical lattices (the reference list cannot be complete bearing in mind that more than 70 papers with "optical lattice" in the title were listed in the cond-mat archive last year only).

At the same time a number of groups [14–18] tried to understand the details of the very first experiment [4] to check the underlying physics. To imagine the difficulty in modeling the experiment let us recall that it involves about 10^5 interacting atoms (bosons) placed in a harmonic trap and a three-dimensional (3D) lattice potential. Such a system is well described by the Bose-Hubbard model with position-dependent chemical potential [1]. Even finding the ground state of the system for that number of particles and $65\times65\times65$ lattice sites is a formidable task. State of the art quantum Monte Carlo (QMC) [14,15,17] calculations aimed at the ground-state properties include up to $16\times16\times16$ sites in 3D [14]; more sites may be included in one- (1D) or two- (2D) dimensional models [15,17]. These studies, while interesting on their own, can shed little light on the *dynamics* of the system when its parameters are varied. Except for special exactly solvable models, the efficient simulation of the time-dependent properties of interacting many-body systems remains an open problem although recently some progress has been obtained for 1D systems [19–21].

It seems, therefore, that the only reasonable and tractable way of analyzing the dynamics of the discussed experiment is using approximate methods. To this end we shall use an approach based on the time-dependent variational principle with the Gutzwiller ansatz. That will allow us to model the details of the 3D experiment [4]. The price for this is similar to that paid in other approximate treatments—one may always question the extent to which the approximations allow one to describe the properties of the systems studied. We hope to convince the reader that the numerical results are at least mutually consistent and thus may provide considerable insight into the dynamics of the experiment.

The discussion of the dynamics is postponed to Sec. III since we discuss in the next section the static mean-field solutions for the ground state for experimental parameters. Here a comparison with available exact QMC results is possible at least. This will give us some confidence about the applicability of the mean-field approach yielding, at the same time, the initial state for the dynamics studied later.

II. STATIC MEAN FIELD FOR THE BOSE-HUBBARD MODEL

The Bose-Hubbard Hamiltonian describing the system takes the form [1]

$$H = -J\sum_{\langle i,j\rangle} a_i^\dagger a_j + \frac{U}{2}\sum_i n_i(n_i-1) + \sum_i W_i n_i, \qquad (1)$$

where $n_i = a_i^\dagger a_i$ is the occupation number operator at site i (with a_i being the corresponding annihilation bosonic operator), U the interaction energy, J the tunneling coefficient, and W_i the energy offset at site i. $\Sigma_{\langle i,j\rangle}$ denotes the sum over nearest neighbors. Both J and U are functions of the lattice potential and may be easily expressed in terms of integrals of the Wannier functions of the lowest energy band for the cold-atom implementation of the model [1].

Consider first the standard homogeneous situation in which all W_i's are equal. The last term in Eq. (1) becomes proportional to the (conserved) number of bosons and may be dropped. The only remaining parameter of the model is the ratio U/J. When tunneling dominates the system, its ground state is superfluid while in the opposite case it becomes a Mott insulator. The borderline between the two phases depends on the chemical potential μ. The Mott insulator state is incompressible and is characterized by an integer mean occupation of sites. In effect starting from the superfluid at small U/J and a noninteger ratio of N/M (N denotes the number of atoms while M is the number of sites)

and increasing U/J the ground state remains superfluid up to the highest values of U/J at fixed boson density. On the other hand the range of μ values corresponding to the commensurate filling increases with U/J. In effect, the separation line between a MI and a SF forms characteristic lobes [2,3,16].

For a detailed discussion of the BH model see [2,16]. As we are interested in the mean-field approximation, let us just quote Zwerger [16] saying "In two- and three-dimensional lattices, the critical value for the transition from a MI to a SF is reasonably well described by a mean-field approximation." In one dimension the mean-field approximation is much worse [16].

In the presence of an additional potential, e.g., a harmonic trap, local energies W_i depend on the site location. Then the effective chemical potential at each site becomes $\mu_i=\mu-W_i$. As pointed out already in [1] this will lead for large U/J to a shell-like structure with MI phases with different integer occupations (highest in the middle, assuming an attractive binding additional potential) separated by SF regions. This picture has been nicely confirmed in quantum Monte Carlo calculations both in 1D [15] and in 3D [14].

The latter exact results are of particular interest for us since they allow for a comparison with the mean-field approximation. In [14] a 3D $16\times16\times16$ lattice is considered with different values of U and J parameters as well as the harmonic trap. To find the mean-field ground state we minimize

$$\langle E\rangle = \langle G|H-\mu\hat{N}|G\rangle, \tag{2}$$

where $\hat{N}=\Sigma_i n_i$ and $|G\rangle$ is the Gutzwiller trial function

$$|G\rangle = \prod_{i=1}^{M}\left(\sum_{n=0}^{n_m} f_n^{(i)}|n\rangle_i\right). \tag{3}$$

The number of parameters $f_n^{(i)}$ depends on the number of sites (here 16^3) as well as the maximal occupation at a given site n_m. The average maximal occupation at the center of the trap is 2 for the data considered in [14]. Therefore, it is sufficient to take $n_m=7$. That yields a minimization procedure over 32 768 parameters. Such a number of parameters must lead to spurious local minima, unless a very good estimate exists for the initial set of $f_n^{(i)}$'s (i.e., the initial $|G\rangle$). Fortunately such a guess is quite obvious and is often termed the local mean-field approximation; namely, at each site i one takes a solution for $f_n^{(i)}$'s corresponding to the homogeneous BH model with the effective chemical potential $\mu_i=\mu-W_i$. Provided W_i changes smoothly from site to site, such an approach should be an excellent approximation to a full mean-field solution. And indeed it is; we have found for the data discussed below that the initial and final $\langle E\rangle$ [see Eq. (2)] differ by at most 2%; the number of iterations of standard *Numerical Recipes* minimization packages [22] is slightly bigger than the number of parameters.

The results obtained are presented in Fig. 1 in the same form as the corresponding plot in [14] to make the comparison easier. The values of parameters correspond to those taken in [14]. The notation used by us differs slightly from

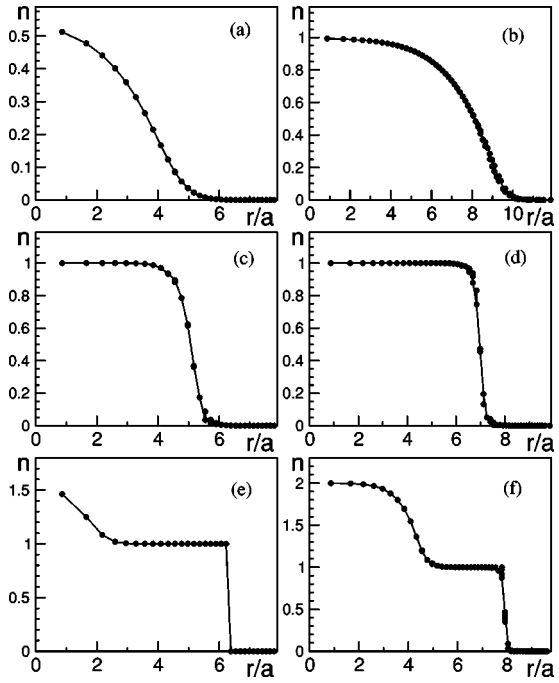

FIG. 1. Mean-field particle density distribution (on-site filling factors) as a function of the distance from the center of the trap measured in units of the lattice constant a. Filled circles correspond to numerical results, lines are drawn to guide the eye. The parameters of the BH model match those quoted in Fig. 1 of [14]; see the text for numerical values. Comparison with the latter results obtained within the "exact" quantum Monte Carlo simulation reveals the accuracy of the mean-field approximation.

that of [14], in particular the tunneling constant J is denoted as t in [14]. For the purpose of this figure all parameters are expressed in units of J, i.e., $J=1$. To make the comparison with notation used in [14] easier, the coefficient in the term proportional to the number of atoms at a given site in Eq. (2), i.e., the difference of the on-site energy W_i and the chemical potential μ is expressed as $W_i-\mu=-U_0+U/2+\kappa\mathbf{x}_i^2$, where $\mathbf{x}_i$ is the position vector of site i with $\mathbf{x}_i^2$ being the square of the distance of the ith site from the center of the harmonic trap measured in units of the lattice constant. With such a definition the parameters used in Fig. 1 take the following values: (a) $U=24.0$, $U_0=-11.08$, $\kappa=0.195\,31$; (b) $U=32.0$, $U_0=-28.08$, $\kappa=0.195\,31$; (c) $U=80.0$, $U_0=-65.0$, $\kappa=0.976\,56$; (a) $U=80.0$, $U_0=-90.0$, $\kappa=1.030\,62$; (a) $U=80.0$, $U_0=-120.08$, $\kappa=2.003\,75$; and (a) $U=80.0$, $U_0=-150.0$, $\kappa=1.757\,81$. A comparison of Fig. 1 with Fig. 1 of [14] indicates that, as far as the average occupation at different sites is concerned, the mean-field solution is in excellent agreement with the quantum Monte Carlo results.

Instead of the occupation at different sites one may take a look at the momentum distribution, i.e., a quantity closely related to that measured in experiment (see [4] and the discussion below). The momentum distribution is given by [14]

$$n_{\mathbf{k}} = |\phi(\mathbf{k})|^2\sum_{i,j} e^{i\mathbf{k}\cdot(\mathbf{r}_i-\mathbf{r}_j)}\langle a_i^\dagger a_j\rangle, \tag{4}$$

where $\mathbf{k}$ is the wave vector and $\phi(\mathbf{k})$ the Fourier transform of the Wannier site function. The latter yields a broad bell-

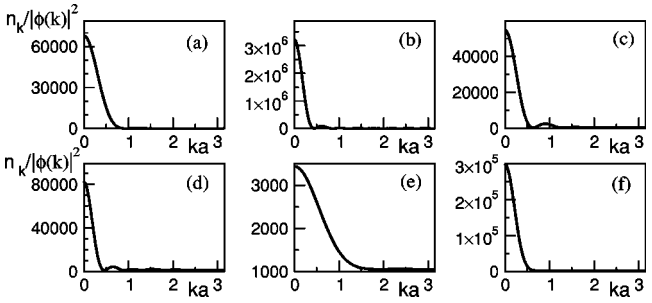

FIG. 2. The rescaled mean-field momentum distribution (in arbitrary units) in the first Brillouin zone in the (0,0,1) direction derived from Eq. (4) for data presented in Fig. 1. The distributions are to be compared with the corresponding "exact" distributions in Fig. 2 of [14]. Observe that the mean-field result differs from the exact distribution for the case (d) only—see discussion in the text.

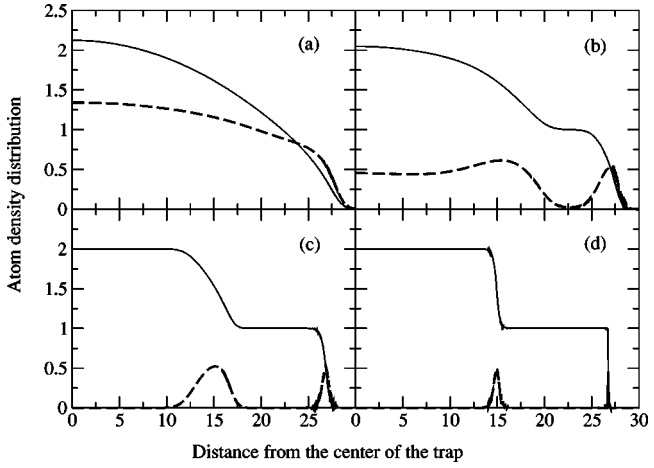

FIG. 3. Solid lines represent mean-field atom density distribution (on-site filling factor n) as a function of the distance from the center of the trap (measured in units of the lattice constant). Dashed lines represent the corresponding variances at different sites $2\sigma_i^2 = 2(\langle n_i^2\rangle - \langle n_i\rangle^2)$. The total number of atoms and the SF factor γ_{SF} (see text) for each plot are (a) $V=9E_r$, $N=99\,771$, $\gamma_{\mathrm{SF}}=0.95$; (b) $V=13E_r$, $N=99\,502$, $\gamma_{\mathrm{SF}}=0.40$; (c) $V=16E_r$, $N=95\,408$, $\gamma_{\mathrm{SF}}=0.11$; (d) $V=22E_r$, $N=94\,172$, $\gamma_{\mathrm{SF}}=0.01$. Small indents seen in the lines in (c) and (d) are due to anisotropy induced by a cubic lattice in an isotropic (harmonic) trap; for further details see text.

shaped background and merely provides information about the lattice. The relevant information about the atoms is contained in the Fourier transform of $\langle a_i^\dagger a_j\rangle$. In the mean-field approximation this factorizes for different i,j as $\langle a_i^\dagger a_j\rangle \approx \langle a_i^\dagger\rangle\langle a_j\rangle$. Such a factorization seems quite drastic and one may expect significant differences between the momentum distributions obtained from QMC simulations and within the mean-field approximation. It is really not so, however, for bosons in a harmonic trap as visualized in Fig. 2 for the mean field. That figure should be compared with QMC results presented in Fig. 2 of [14]. Observe that differences appear only for Fig. 2(d), the exact results yielding a significantly broader momentum distribution. As discussed in [14] almost no SF fraction is present in the QMC result corresponding to Fig. 2(d). Then the factorization must affect strongly the momentum distribution since in a vast majority of sites $\langle a_i\rangle = 0$. Clearly, however, as long as some SF fraction is present in the system the mean-field momentum distribution closely resembles the exact quantum results.

This apparent quite close agreement between QMC results and the mean-field approximation for a $16\times16\times16$ lattice and about 10^3 atoms is very encouraging in view of the realistic experimental conditions [4]. Here both the external potential changes less rapidly (the size of the lattice is now $65\times65\times65$) and the number of atoms exceeds 10^5; thus one may expect that the mean-field approximation works even better.

While the test described above has been performed for some values of U, J, as well as the trap frequency, chosen (by the authors of [14]) to simulate the experiment, we have to determine first the relevant range of parameters. From now on we shall measure quantities of the dimension of energy in units of the recoil energy of ^{87}Rb atoms for light with a wavelength $\lambda = 2\pi/K = 852$ nm, i.e., $E_r = \hbar^2K^2/2M$, where M is the mass of ^{87}Rb atoms. The depth of the optical lattice V changes from 0 to $22E_r$. Finding Wannier functions for different values of V [23], we evaluate the corresponding $U(V)$ and $J(V)$ values. The energy offset at each site W_i has two components in the experiment [4]. One is the harmonic magnetic trap potential (time independent); the other is due to the Gaussian intensity profiles of the lattice-creating laser beams. The latter may also be approximated by a harmonic term [4]; the corresponding frequency is then dependent on V.

To find the mean-field ground state for different V values and the number of atoms of the order of 10^5 one needs to solve a minimization problem over 2×10^6 parameters (with $n_m=7$ as before) which is hardly manageable. One may, however, use the symmetry of the problem (cubic lattice combined with spherically symmetric trap) to significantly reduce that number. Let i,j,k count the sites in the x,y,z directions, respectively, with each index taking values from -32 to $n_s=32$ (yielding 65 sites in each direction). Due to the ground-state symmetry it is enough to consider only the sites with $0\leqslant i\leqslant j\leqslant k\leqslant n_s$ which reduces the number of minimized parameters to about 48 000. Needless to say we have checked on the smaller $16\times16\times16$ problem that the symmetry-reduced problem yields the same ground state as the full minimization.

The results obtained are presented in Fig. 3 and are practically indistinguishable from the initial guess, i.e., the wave function coming from the local mean-field approximation discussed above. The chemical potential μ has been adjusted (for each case) to have the average number of atoms $N = \langle\hat{N}\rangle = \Sigma_i\langle n_i\rangle$ around 10^5. This leads to more than two atoms (on average) per site in the center of the trap. To characterize whether the state is closer to being superfluid or Mott insulator we define the superfluid factor $\gamma_{\mathrm{SF}} = (1/N)\Sigma\langle a_i\rangle\langle a_i^\dagger\rangle$. This factor is zero for a pure MI state (when $\langle a_i\rangle = 0$ as each node is in a Fock state) and reaches unity for Poissonian statistics at each node. While obviously it is not a "proper" order parameter for the phase transition, it seems to be convenient for characterizing the states obtained. Using this factor we can quantify the states shown in Fig. 1, noting first a

general qualitative agreement with the experimental findings [4]. The case $V=9E_r$ seems almost fully superfluid (with, however, strongly sub-Poissonian statistics [24] at each site), the case $V=13E_r$ shows the first traces of the insulator phase (integer occupation of sites with vanishing variance), the transition is completed for a significant fraction of sites at $V=16E_r$, while for the deepest lattice $V=22E_r$ the SF fraction is restricted to very narrow regions separating different integer occupations. A careful reader may notice small indents visible in the lines in Figs. 3(c) and 3(d). They are due to anisotropy induced by the cubic lattice on the isotropic harmonic trap. The data, presented necessarily as a function of the radial distance, contain occupations along the axes, the diagonals, and other nonequivalent directions in the cubic lattice. The smallness of the indents indicates that the symmetry of the trap is dominant.

III. TIME-DEPENDENT MEAN-FIELD DYNAMICS

The results obtained for the mean-field ground state in realistic situations, shown in the previous section, seem quite encouraging. Yet, in themselves, they can say little about the dynamics of the system when the lattice depth V is varied. In an attempt to address this important issue we shall use a time-dependent version of the mean-field approximation. To this end we employ the time-dependent variational principle [8] looking for the minimum of

$$\left\langle G(t)\left| i\hbar\frac{\partial}{\partial t} - H(t) + \mu\hat{N}\right| G(t)\right\rangle, \tag{5}$$

with $H(t)$ being now the time-dependent Hamiltonian. The time dependence is implicit via the dependence of the BH Hamiltonian H on U, J, and W_i, which in turn depend on V. The chemical potential μ becomes also time dependent when the system parameters are varied. $|G(t)\rangle$, the variational wave function, is assumed in the standard Gutzwiller-type form (3), with $f_n^{(i)}(t)$ now being time dependent. The very same approach has been successfully applied recently to the formation of molecules [8,9], the treatment of disordered optical lattices [10], and for determining the phase diagram in Bose-Fermi mixtures [13].

The minimization of (5) yields a set of first-order differential equations for $f_n^{(i)}(t)$:

$$i\frac{d}{dt}f_n^{(i)} = \left[\frac{U}{2}n(n-1) + n(W_i-\mu)\right]f_n^{(i)} - J[\Phi_i^{\star}\sqrt{n+1}f_{n+1}^{(i)} + \Phi_i\sqrt{n}f_{n-1}^{(i)}], \tag{6}$$

where $\Phi_i=\Sigma_{\langle j\rangle}\langle G(t)|a_j|G(t)\rangle$ (the sum, as indicated by the subscript in angular brackets is over the nearest neighbors only). The nice feature of the evolution resulting from Eq. (6) is that the average number of particles $N=\langle\hat{N}\rangle$ is an exact constant of the motion [8]. Naturally, when the parameters of the BH model, e.g., U and J, change the chemical potential corresponding to the mean-field solution with a given number of particles N also changes. The dynamics of μ cannot be obtained from Eq. (6) only. One can find it, however, by following the evolution of two states $|G_1\rangle$ and $|G_2\rangle$ with slightly different average numbers of particles $N_2=\langle G_2|\hat{N}|G_2\rangle=N_1+\delta N=\langle G_1|\hat{N}|G_1\rangle+\delta N$. The chemical potential at given t may be then approximated by $\mu(t)=[\langle G_2(t)|H(t)|G_2(t)\rangle-\langle G_1(t)|H(t)|G_1(t)\rangle]/\delta N$ and adjusted at each time step [13]. This is the approach used in the numerical results presented below.

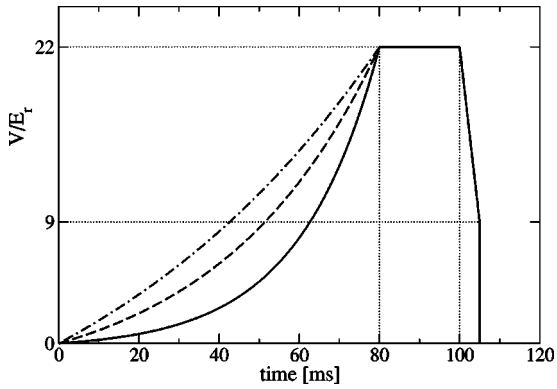

FIG. 4. The experimental time profile (solid line) of the lattice potential depth V measured in recoil energy E_r units. The initial exponential increase with a time constant $\tau=20$ ms is followed by a flat part and a subsequent decrease to $V_f=9E_r$ with a linear ramp with varying slope. Dashed line corresponds to the exponential time constant $\tau=40$ ms, dash-dotted to $\tau=80$ ms. Thin dotted lines indicate particularly interesting values of time and V—see text for discussion.

Since we want to follow as closely as possible the experiment [4] let us recall its main features. The experiment has three stages after loading the harmonic trap with Rb condensate—compare Fig. 4. First, the optical lattice depth $V(t)$ was increased in 80 ms (using an exponential ramp with time constant $\tau=20$ ms) from the initial zero value (when the harmonic trap was present only) to $V_{\max}=22E_r$, where E_r is the recoil energy of Rb atoms. The sample was then held for 20 ms at $V_{\max}$. Finally $V(t)$ was decreased with a linear ramp to $V_f=9E_r$ with different speed. At any stage the experiment could be interrupted by rapidly switching off all laser beams building up the lattice as well as the magnetic trap. The freely expanding atomic cloud, after some delay, was recorded by destructive absorption imaging, yielding a signal that reflects the momentum distribution [14,16]. Since the absorption images are taken along two orthogonal axes the quantity measured is in fact the integrated momentum distribution [14]

$$N(k_x,k_y) \propto \int dk_z n_{\mathbf{k}}. \tag{7}$$

For clouds released from low optical lattices when tunneling dominates and the superfluid behavior is expected the signal reflects Bragg peaks due to interferences of atoms coming from different lattice sites. At increased lattice depths above $13E_r$ the interference maxima become immersed in an incoherent background practically disappearing at $20E_r$. This behavior was associated with the quantum phase transition from the SF to the MI phase [4]. Most interestingly, the coherence of the sample may be rapidly recov-

ered when the lattice depth is decreased (third stage of the experiment) as measured by the width of the central interference peak which decreases almost to its original value at $V=9E_r$ in about 4 ms.

In former applications of the time-dependent mean-field approach [8–10,13] the time dependence of the system's parameters was assumed to be sufficiently slow to assure adiabaticity. In effect the mean-field ground state has been followed by applying the time-dependent equations for the $f_n^{(i)}(t)$'s [Eq. (6)]. Here we have a similar situation since it is claimed [4] that the changes in time of $V(t)$ are made sufficiently slow to keep the system in the many-body ground state. Having the mean-field ground states for different V values we can (within the mean-field approximation) test this adiabaticity assumption.

Looking again at the time profile depicted in Fig. 4 one may notice that the ramp used in the experiment leads indeed to a very slow increase of $V(t)$ initially; however, changes of $V(t)$ become relatively rapid about and above $V=9E_r$, i.e., in the region where the transition from SF to MI is supposed to take place. Taking as the initial state the mean-field ground state at $V=9E_r$, our simulations show that to assure adiabaticity a small change of V on the superfluid side (say from $V=9E_r$ to $9.1E_r$) requires about 20 ms (one needs 40 ms for a loop from $V=9E_r$ to $9.1E_r$ and back to keep the overlap with the initial state of the order of 99%). That strongly indicates that a much longer time is needed to traverse adiabatically the whole interesting region from $V=9E_r$ to $22E_r$. And that change is realized in about 20 ms in the experiment.

To test the adiabatic issue further we shall concentrate in the following on the regime above $V=9E_r$ containing the quantum phase transition. Starting again from the Gutzwiller mean-field ground state at $V=9E_r$ we simulate the time evolution up to $V=22E_r$ (with experimental time profile). We may compare the dynamically obtained wave function plotted in Fig. 5(a) with the mean-field ground state at $V=22E_r$ [Fig. 5(d)]. While the ground state has an insulator character almost everywhere in the trap with $\gamma_{\mathrm{SF}}=0.01$, the dynamically evolved wave function, by comparison, seems to reflect an excited wave packet and it has rather small regions where the occupation of sites is close to integer with vanishing number variance. The corresponding $\gamma_{\mathrm{SF}}=0.12$ confirms the presence of a relatively large superfluid region.

To show that the effect is really due to the too fast increase of the lattice depth we have modified the experimental time profile slightly, by changing the exponential constant τ from 20 to 40 ms (or 80 ms). That makes the initial rise of the laser intensity (and the lattice depth) more uniform in time (compare Fig. 4). Observe that while the full duration of the first stage remains the same, the interval of time spent on the increase of the lattice depth from $V=9E_r$ to $22E_r$ increases from below 20 ms (experimental profile), to about 30 ms (for $\tau=40$ ms) or about 37 ms (for $\tau=80$ ms). Starting again from the mean-field ground state at $V=9E_r$ we obtain the atom density profiles shown in Figs. 5(b) and 5(c), respectively. Observe that the regions of insulator behavior for both cases are much larger than observed previously. The corresponding superfluid factors are $\gamma_{\mathrm{SF}}=0.062$ for $\tau=40$ ms and $\gamma_{\mathrm{SF}}=0.048$ for $\tau=80$ ms. While the final distributions still show signs of significant excitations, the insulator character becomes dominant for Fig. 5(c) and also for Fig. 5(b).

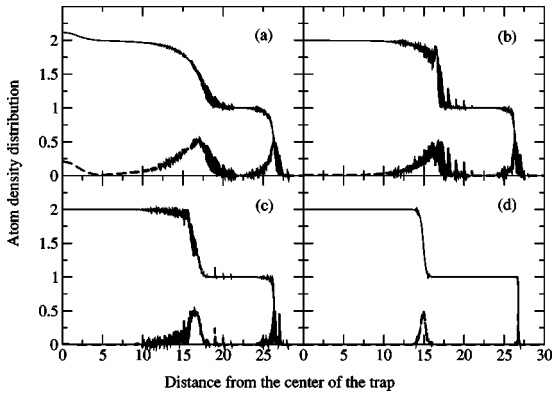

FIG. 5. Atom density distribution (on-site filling factor) after a mean-field evolution starting from the mean-field ground state at $V=9E_r$ at the final value of $V=22E_r$ for different $V(t)$ time dependence. Exponential time scale of (a) 20, (b) 40, and (c) 80 ms. The longer the time scale, the slower the change of $V(t)$ in the considered range as can be seen in Fig. 4. Thick dashed lines in (a)–(c) present twice the variance of the on-site occupation showing that the insulator regions in (b) and (c) are much larger than in (a). (d) repeats, after Fig. 3, the mean-field ground state at $V=22E_r$ for comparison. Observe that indents in the lines for dynamically evolved wave functions are much more pronounced than in the static (d) case. As before these indents are due to different symmetries of the cubic lattice and spherically harmonic isotropic trap. The conflicting symmetries lead to anisotropic excitations in the dynamical situations when the potential parameters are varied. Those excitations are responsible for the indents.

Keeping the overall duration of the laser intensity turn-on at 80 ms and enlarging the final stage comes at the price that the initial rise from $V=0E_r$ to $V=9E_r$, very smooth in the experiment [4] for $\tau=20$ ms, becomes sharper for larger τ (compare Fig. 4). Thus larger τ may lead to some excitation at the initial creation of the lattice, not apparent in our simulations since we start from the ground state at $V=9E_r$. Trying to keep the total duration of the experiment as short as possible (to avoid, for example, decoherence) one can still imagine a slightly more sophisticated pulse rise with say $\tau=20$ ms initially up to say $V=9E_r$ and further increase with a larger time constant, say 40 ms. While the duration of the experiment increases by 10% only, the degree of excitation of the final wave packet becomes much smaller and the insulator character much more pronounced.

In the experiment [4] the atomic density distribution is not measured directly. The presence of the Mott insulator layer was detected by observing the resonance in the excitation spectrum around the interaction energy U. Clearly the size of the corresponding peak is related to the number of atoms in the insulator layers. Our results indicate that an appropriate suggested change in the time profile of $V(t)$ should increase the size of insulator regions and thus enhance the resonant peak in the excitation spectrum.

Let us mention also that qualitatively similar results to those depicted in Fig. 5 are obtained starting the evolution

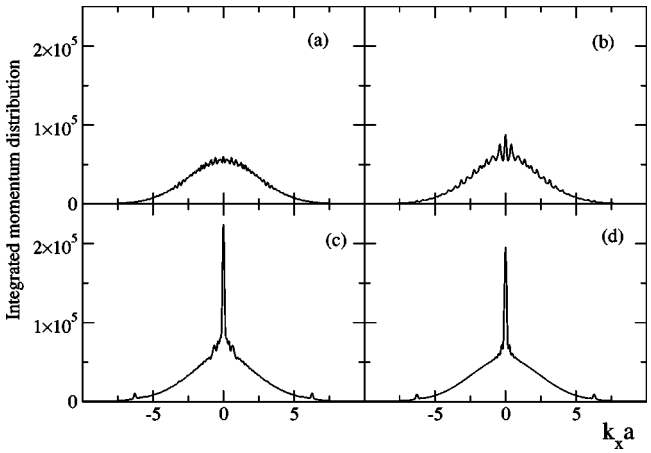

FIG. 6. Integrated momentum distributions (7) for states shown in Fig. 5 (panels match one another). The cut $N(k_x,0)$ along $k_y=0$ is shown only. Observe that for the time profile of the experiment no narrow peak is visible, in agreement with the experiment. For a more adiabatic time scale (c) as well as for the ground state (d) a narrow peak in the momentum distribution is clearly visible. For further discussion see text.

from different value of V, say $V=8E_r$, as long as the initial V is sufficiently big but smaller than the beginning of the SF-MI transition regime (around $V=13E_r$). In the experiment the lattice depth is increased from the initial zero value but for that case the Bose-Hubbard Hamiltonian (1) is not a good model to describe the cold-atom physics. This discrete lattice model is appropriate [1,16] when the atoms have to remain in the lowest vibrational state at each site, that is, for a sufficiently deep lattice.

It is most interesting to compare the integrated momentum distributions (7) corresponding to the position distributions shown in Fig. 5. The cuts along $k_y=0$ are presented in Fig. 6. In contrast to Fig. 2 we include now the Fourier transform of the Wannier function [compare Eq. (4)] so the quantity plotted matches the experiment (for a better quantitative picture, we prefer the cut along $k_y=0$ instead of the three-dimensional color plot used originally to represent the experimental data). Figure 6(a) corresponds to the experimental profile. Observe that the integrated momentum distribution consists of a broad peak in a very nice agreement with the experiment [4]. Note, however, that for other, "more adiabatic" time profiles the narrow central structure emerges [compare Fig. 6(b)] becoming quite pronounced both for Fig. 5(c) as well as for the mean-field ground-state momentum distribution—depicted in Fig. 6(d). The absence of the narrow Bragg peak in the experiment seems to be, therefore, not related to the emergence of the insulator phase as suggested in [4]. The persistence of the narrow peaks in the Mott regime has been already noted in [14] in a model static quantum Monte Carlo study on a smaller lattice. The result presented in Fig. 6(d) indicates that the conclusion of the authors [14] concerning the ground-state momentum distribution extends also to a realistic sample. The dynamical results presented in Fig. 6 suggest that fading of the Bragg peaks and the appearance of the broad integrated momentum distribution can be associated with a significant excitation of the sample rather than the transition to the Mott insulator regime.

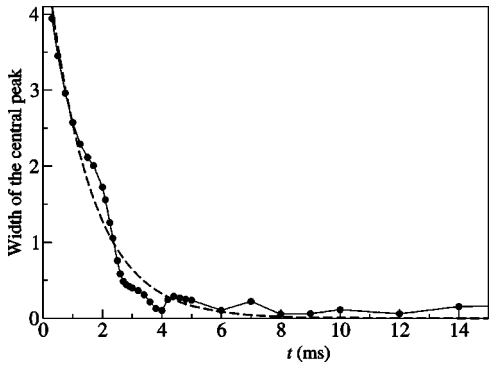

FIG. 7. Half-width of the central interference peak for different ramp-down times t_r obtained by a Lorentzian fit of the integrated momentum distribution—compare Eq. (7). Filled circles are connected by a line to guide the eye. Dashed line is a single-exponential decay with a time constant $\tau=1.45$ ms.

The reliability of the dynamical mean-field approach may be tested further in an attempt to reproduce the "restoration of coherence" part of the experiment [4]. In the experiment, after reaching $V=22E_r$ the lattice depth is kept constant for 20 ms and then decreased back to $V=9E_r$ with a linear ramp of duration t. It is shown that the time needed to restore the narrow interference pattern in the integrated momentum distribution is of the order of 4 ms. This phenomenon is associated with restoring the coherence in the sample.

This *interpretation* is in contradiction with results already presented in Fig. 6—the existence (or the lack of it) of the narrow peaks seems not to be solely related to the coherence of the sample but also to its excitation. The question, however, remains whether the dynamical mean-field calculation can reproduce the *results* of the experiment, i.e., the dependence of the width of the interference pattern on the time duration of lowering the lattice.

To answer this question we make a simulation (the results are shown in Fig. 7), starting from the static solution in the SF regime (taken for convenience at $V=9E_r$ again) increasing the lattice height exponentially as in the experiment [4], the subsequent delay of 20 ms at $V=22E_r$, and a linear ramp down with various slopes. Note that the shape of the curve as well as the time scale of restoring the narrow interference pattern are in quite good agreement with the experiment. While the experimental data could be fitted with a double-exponential decay with two time scales, our mean-field data are reasonably reproduced with a single-exponential decay with time scale $\tau=1.45$ ms. This nicely corresponds with the shorter time scale of the experiment (0.94 ms). The obtained time scale is also of the order of a typical single tunneling time ($1/J$ in appropriate units) to a nearby site. Our numerical data fail to reproduce the second experimental time scale. This points to the possibility that it can be associated indeed with a long-range correlation between sites. Such a a long-range correlation should not manifest itself in our mean-field simulations—the Gutzwiller wave function neglects entanglement between sites.

The observed quite good agreement of the obtained widths of the momentum distribution with the experiment [4]

seems to be quite a spectacular success of the dynamical mean-field simulation bearing in mind its simplicity. The fact that the mean-field approach works so well may be, in our opinion, attributed to the fact that the dynamics takes place in the regime where the superfluid fraction remains significant. Then the mean atomic field Φ_i does not vanish, allowing for a semiclassical (mean-field) description. Our results suggest that the system has quite a long memory and remembers that it was originally a SF. This fits nicely with the excited wave-packet-like character of the dynamically obtained wave function clearly visible in Fig. 5(a).

IV. CONCLUSIONS

To summarize, it has been shown that the mean-field Gutzwiller approximation allows one to simulate the dynamics of the inhomogeneous Bose-Hubbard model taking into account realistic experimental conditions. The accuracy of the approximation cannot be controlled, which is the major drawback of the present approach (a comparison with exact dynamics for small systems will lead us nowhere since then the mean-field approach is known to fail). On the other hand a comparison with the available data seems quite encouraging. Accepting mean-field predictions, we may confirm that indeed the transition from superfluid to Mott insulator takes place (albeit in a small part of the sample) in the experiment [4]. On the other hand, the claim that the first stage of the experiment is performed adiabatically assuring that the system remains in its many-body ground state (and thus a genuine textbook quantum phase transition [3] is realized) seems questionable. We confirm the suggestion of [14] that fading of narrow peaks in the momentum distribution should not be associated with the transition to the Mott insulator regime. Rather it is a dynamical effect.

We suggest that optimization of the lattice-depth time dependence (i.e., laser intensity profile) may help to enlarge the insulator regions, making the transition more adiabatic. That may be detected by measuring the size of the peak in the excitation spectrum of the system.

Note added. Recent work [25] reports a study of the exact dynamics of the model using the method of [20,21]. However, the results consider at most 49 atoms in 40 sites of a 1D lattice.

ACKNOWLEDGMENTS

Participation of D. Delande at the early stage of this work is appreciated as well as discussions with B. Damski, M. Lewenstein, and K. Sacha. This work was supported by the Polish Committee for Scientific Research Grant Quantum Information and Quantum Engineering Grant No. PBZ-MIN-008/P03/2003.

[1] D. Jaksch, C. Bruder, J. I. Cirac, C. W. Gardiner, and P. Zoller, Phys. Rev. Lett. **81**, 3108 (1998).
[2] M. P. A. Fisher, P. B. Weichman, G. Grinstein, and D. S. Fisher, Phys. Rev. B **40**, 546 (1989).
[3] S. Sachdev, *Quantum Phase Transitions* (Cambridge University Press, Cambridge, U.K., 2001).
[4] M. Greiner, O. Mandel, T. Esslinger, T. W. Hänsch, and I. Bloch, Nature (London) **415**, 39 (2002).
[5] D. van Oosten, P. van der Straten, and H. T. C. Stoof, Phys. Rev. A **63**, 053601 (2001).
[6] D. B. M. Dickerscheid, D. van Oosten, P. J. H. Denteneer, and H. T. C. Stoof, Phys. Rev. A **68**, 043623 (2003).
[7] C. Menotti, A. Smerzi, and A. Trombettoni, New J. Phys. **5**, 112 (2003).
[8] D. Jaksch, V. Venturi, J. I. Cirac, C. J. Williams, and P. Zoller, Phys. Rev. Lett. **89**, 040402 (2002).
[9] B. Damski, L. Santos, E. Tiemann, M. Lewenstein, S. Kotochigova, P. Julienne, and P. Zoller, Phys. Rev. Lett. **90**, 110401 (2003).
[10] B. Damski, J. Zakrzewski, L. Santos, P. Zoller, and M. Lewenstein, Phys. Rev. Lett. **91**, 080403 (2003).
[11] A. Albus, F. Illuminati, and J. Eisert, Phys. Rev. A **68**, 023606 (2003).
[12] H. P. Büchler and G. Blatter, Phys. Rev. Lett. **91**, 130404 (2003).
[13] H. Fehrmann, M. A. Baranov, B. Damski, M. Lewenstein, and L. Santos, e-print cond-mat/0307635.
[14] V. A. Kashurnikov, N. V. Prokof'ev, and B. V. Svistunov, Phys. Rev. A **66**, 031601 (2002).
[15] G. G. Batrouni, V. Rousseau, R. T. Scalettar, M. Rigol, A. Muramatsu, P. J. H. Denteneer, and M. Troyer, Phys. Rev. Lett. **89**, 117203 (2002).
[16] W. Zwerger, J. Opt. B: Quantum Semiclassical Opt. **5**, S9 (2003).
[17] S. Wessel, F. Alet, M. Troyer, and G. G. Batrouni, Phys. Rev. A **70**, 053615 (2004).
[18] D. C. Roberts and K. Burnett, Phys. Rev. Lett. **90**, 150401 (2003).
[19] L. Amico and V. Penna, Phys. Rev. Lett. **80**, 2189 (1998).
[20] G. Vidal, Phys. Rev. Lett. **91**, 147902 (2003).
[21] A. J. Daley, C. Kollath, U. Schollwöck, and G. Vidal, J. Stat. Mech.: Theory Exp. **2004**, P04005 (2004).
[22] W. H. Preiss, S. A. Teukolsky, W. T. Vetterling, and B. P. Flannery, *Numerical Recipes in Fortran* (Cambridge University Press, Cambridge, U.K., 1996).
[23] Bogdan Damski was very kind to supply the appropriate numerical code.
[24] C. Orzel, A. K. Tuchman, M. L. Fenselau, M. Yasuda, and M. A. Kasevich, Science **291**, 2386 (2001).
[25] S. R. Clark and D. Jaksch, Phys. Rev. A **70**, 043612 (2004).